Versatile Fluorescence Resonance Energy Transfer-Based Mesoporous Silica Nanoparticles for Real-Time Monitoring of Drug Release

Jinping Lai,[†] Birju P. Shah,[†] Eric Garfunkel, and Ki-Bum Lee*

Department of Chemistry and Chemical Biology Institute for Advanced Materials, Devices and Nanotechnology (IAMDN), Rutgers University, Piscataway, New Jersey 08854, United States. [†]These authors have contributed equally to this manuscript.

ABSTRACT

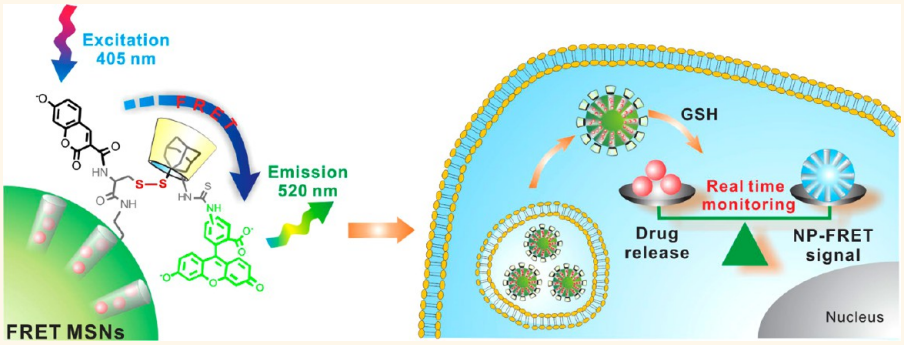

We describe the development of a versatile fluorescence resonance energy transfer (FRET)-based real-time monitoring system, consisting of (a) coumarin-labeled-cysteine tethered mesoporous silica nanoparticles (MSNs) as the drug carrier, (b) a fluorescein isothiocyanate-β-cyclodextrin (FITC-β-CD) as redox-responsive molecular valve blocking the pores, and (c) a FRET donor—acceptor pair of coumarin and FITC integrated within the pore-unlocking event, thereby allowing for monitoring the release of drugs from the pores in real-time. Under nonreducing conditions, when the disulfide bond is intact, the close proximity between coumarin and FITC on the surface of MSNs results in FRET from coumarin to FITC. However, in the presence of the redox stimuli like glutathione (GSH), the disulfide bond is cleaved which leads to the removal of molecular valve (FITC-β-CD), thus triggering drug release and eliminating FRET. By engineering such a FRET-active donor—acceptor structure within the redox-responsive molecular valve, we can monitor the release of the drugs entrapped within the pores of the MSN nanocarrier, following the change in the FRET signal. We have demonstrated that, any exogenous or endogenous change in the GSH concentration will result in a change in the extent of drug release as well as a concurrent change in the FRET signal, allowing us to extend the applications of our FRET-based MSNs for monitoring the release of any type of drug molecule in real-time.

KEYWORDS: drug delivery · real-time monitoring · fluorescence resonance energy transfer · mesoporous silica nanoparticle (MSN)-based drug delivery · stimuli-responsive

It has been known that diseased/injured microenvironments release different biological cues and follow abnormal regulatory cycles when compared to physiologically normal cells and tissues.[1−3] Such dynamic microenvironmental conditions require scientists to develop more effective nanomaterial-based drug delivery systems (DDSs) having the following attributes: (i) they can deliver multiple drugs such as organic small molecules, proteins, peptides, DNA, and RNAi molecules without any physicochemical alterations to drug structure,[4−8] (ii) they can modulate the drug-release profile in response to external or internal stimuli for enhancing therapeutic efficacy and minimizing side-effects of drug treatment,[9−15] and (iii) they can monitor the drug release in real time for investigating accumulation of the drugs at the targeted area.[16−21] In this regard, mesoporous silica nanoparticles (MSNs) have excellent potential as DDSs owing to their unique porous structure, tunable pore size, biocompatibility, ease of surface functionalization, and overall

* Address correspondence to kblee@rutgers.edu.

Received for review January 14, 2013 and accepted February 27, 2013.

Published online February 27, 2013
10.1021/nn400199t

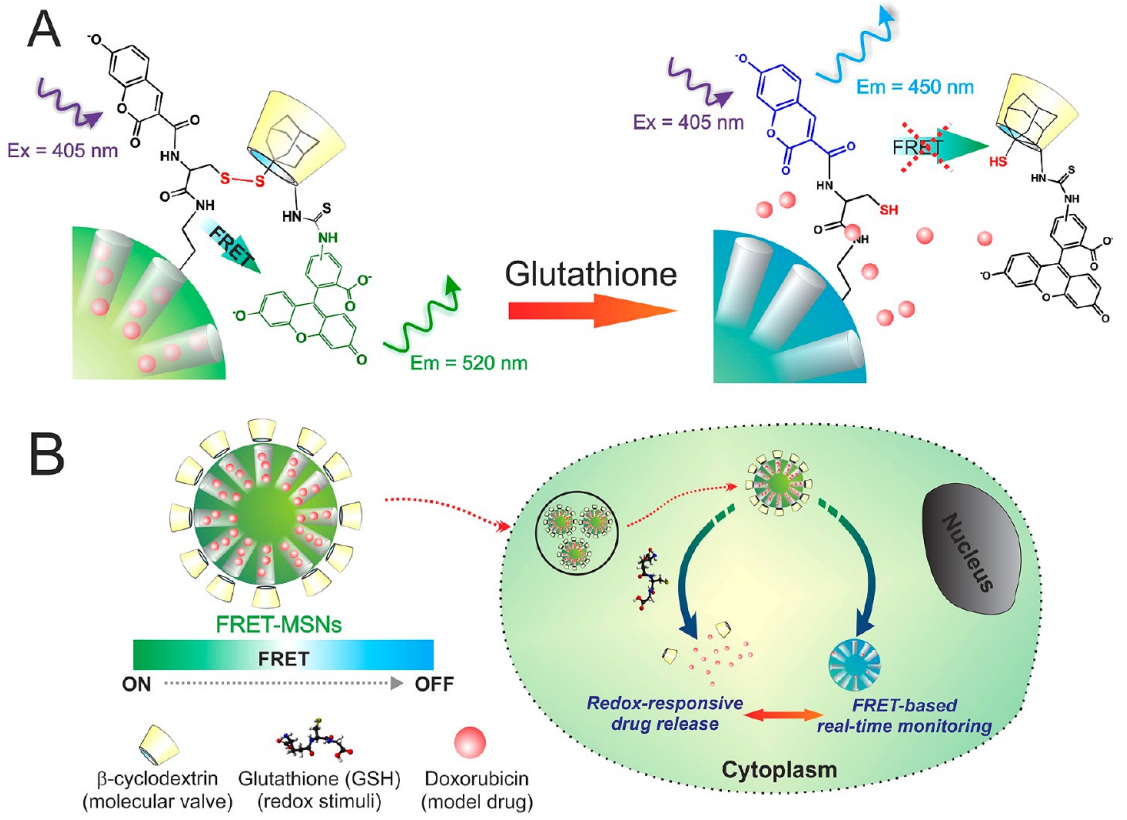

Figure 1. Schematic representation of the redox responsive FRET-MSNs. (A) The coumarin-labeled cysteine on the surface of the FRET-MSNs act as a donor and the FITC-β-CD act as an acceptor, thereby forming a FRET system when the disulfide bond is intact (left). When the disulfide bond is cleaved in the presence of redox stimuli, glutathione, the FITC-β-CD, which also acts as the molecular valve, is removed from the surface of the MSNs, thereby the FRET between coumarin and FITC is abolished. (B) The delivery of encapsulated cargo is selectively triggered in the presence of the redox-stimuli, glutathione which is found in significantly higher amounts in the cytoplasm of cancer cells and the concomitant change of FRET signal can be used to report the uncaging event and estimate the dosing amount of drug. Figure 1A is a magnified representation of Figure 1B, indicating the FRET system.

versatility.[22−24] The hexagonal-ordered pore network within these MSNs allows for entrapping drugs within these pores by simple diffusion. Additionally, the pores can be functionalized with molecular valves designed to trigger the release of the entrapped drugs in the presence of external or internal stimuli including light,[25−29] temperature,[30−32] pH,[33−37] and biomolecules.[38−42] While there have been numerous reports on the design and development of stimuli-responsive MSNs for drug delivery, development of strategies for real-time monitoring of drug release inside the targeted cells is still in its nascent stage. The most widely used among these strategies include using fluorescent dyes/drugs as a model cargo system,[18−35] or conjugating the drugs with caged dyes.[19,20] However, such strategies come with their own limitations such as difficulty in correlating the release of the fluorescent model dye to that of the actual drug molecules; restricting the usage of fluorescent drugs like doxorubicin as model cargoes, although most of the current drug candidates are nonfluorescent; and the possibility of affecting the therapeutic efficacy of the drug owing to structural changes required for conjugation of dyes. Such challenges in investigating the release of drug in complex cellular microenvironments necessitate the development and integration of a real-time monitoring system within the stimuli-responsive nanomaterial-based DDSs.

To address the aforementioned issues, herein we describe the synthesis and development of a redox-responsive fluorescent resonance energy transfer-based MSN drug delivery system (henceforth referred to as FRET-MSN), which enables real-time monitoring (based upon the FRET signal) of redox-responsive drug release occurring in the presence of glutathione found in significantly higher levels in the cancer cells (Figure 1).[43−45] Fluorescence resonance energy transfer (or Förster resonance energy transfer, FRET) is a well-established energy transfer process between two fluorophores which is very sensitive to changes at the nanometer-scale (typically less than 10 nm) in the donor-to-acceptor separation distance.[46] This unique feature of FRET can potentially be an ideal tool to monitor delicate interactions between nanomaterial-based DDSs and external/internal stimuli.[47,48] As illustrated in Figure 1, our FRET-based real-time monitoring platform comprises four components: (i) coumarin (donor)-tethered MSNs as the drug carriers,

(ii) fluorescein isothiocyanate (FITC, acceptor)-attached β-cyclodextrin (β-CD) as the molecular cap to entrap the drugs within the MSNs, (iii) disulfide linkage as the redox-responsive trigger to release the entrapped drug molecules, and (iv) FRET donor–acceptor pair of coumarin and FITC for monitoring drug release in real time. Under nonreducing conditions (*e.g.*, without glutathione),[49] the intact disulfide bond supports formation of a donor–acceptor complex between the coumarin-attached MSN and the FITC-β-CD molecular cap, thereby creating a FRET system. At this stage (FRET ON), the coumarin and FITC moieties are in close proximity on the MSN surface and the FRET-MSNs display an emission peak at 520 nm (correlated to energy transfer from coumarin to FITC), when they are excited at 405 nm (the excitation wavelength of coumarin). However, in the presence of a reducing environment (*e.g.*, with glutathione), the disulfide bond can be cleaved,[49] causing the removal of the FITC-β-CD cap from the MSNs, thereby unlocking the pores and releasing the cargo within. Upon cleavage of the disulfide bond, the FITC-β-CD diffuses away from the MSN surface; hence the FRET between coumarin and FITC is abolished (FRET OFF), and the MSNs display emission at 450 nm (characteristic of coumarin) when excited at 405 nm. Since the on/off change in FRET signal is regulated by molecular structures within our platform and correlated to the unlocking event, we can monitor and quantify the drug release process, by measuring the change of FRET signal. By monitoring the FRET signal on the nanoparticles in real-time, we can visualize the release of any drug molecules, without relying on the drug's optical properties, thereby extending the application of our FRET-MSNs to many drug molecules without compromising their efficacy.

RESULTS AND DISCUSSION

Synthesis and Characterization of FRET-MSNs. The generation of our FRET-MSN-based drug delivery system began with the synthesis of MCM-41type MSNs *via* condensation of tetraethylorthosilicate (TEOS) in the presence of a cetyltrimethylammonium bromide (CTAB) micelle template (Figure 2A).[50] These MSNs were then

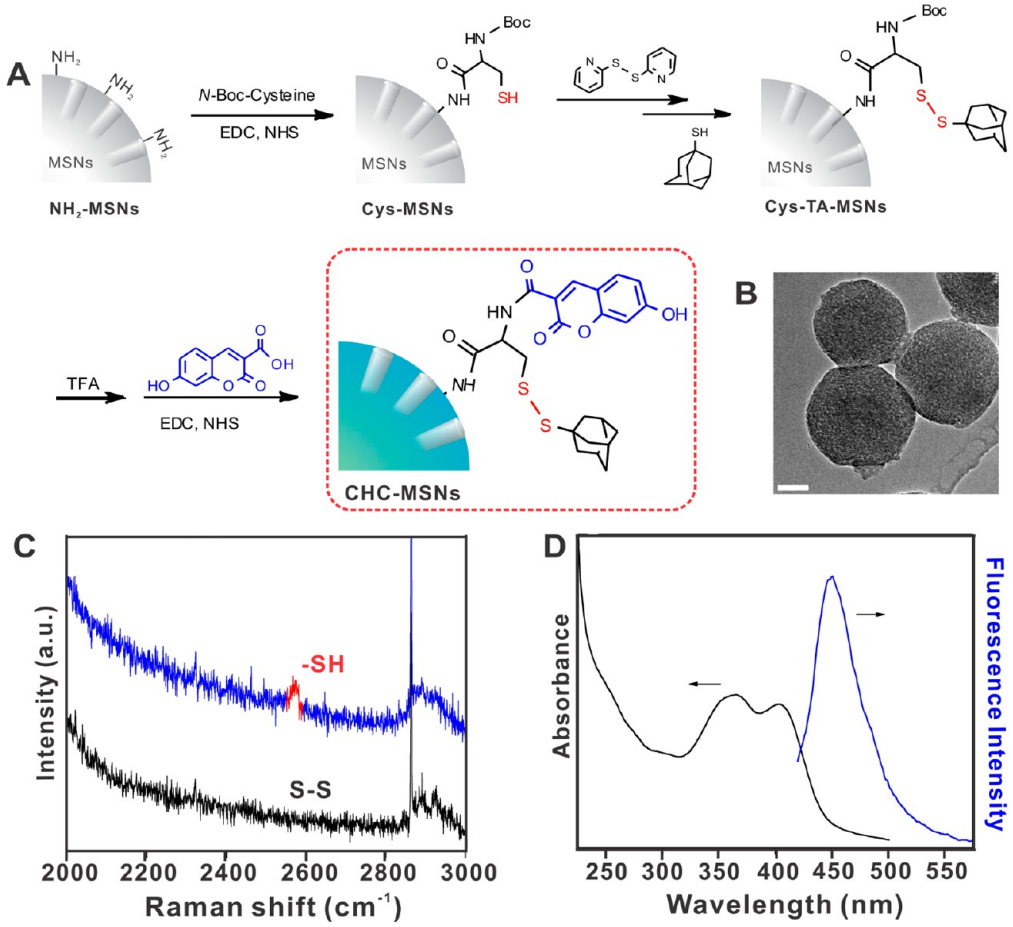

Figure 2. (A) Schematic illustration of the synthesis of CHC-labeled MSNs. The CHC moiety acts as the FRET donor in our FRET-MSNs. (B) TEM image of CHC-MSNs. Scale bar is 50 nm. TEM image confirms that CHC-MSNs retain characteristics typical of MCM-41 type nanoparticles. (C) Raman spectra confirming the formation of a disulfide bond, following conjugation with 1-adamantane thiol. The top curve indicates the free thiol (–SH) moiety on the surface of CHC MSNs, prior to conjugation with 1-adamantanethiol. Following conjugation, no free –SH groups are observed as shown in the bottom curve, thus indicating successful formation of disulfide bond. (D) UV–visible absorbance and emission spectra for CHC-MSNs. The CHC moiety in the CHC-MSNs absorbs maximally at 405 nm and emits light corresponding to 450 nm, thereby acting as a FRET donor for FITC.

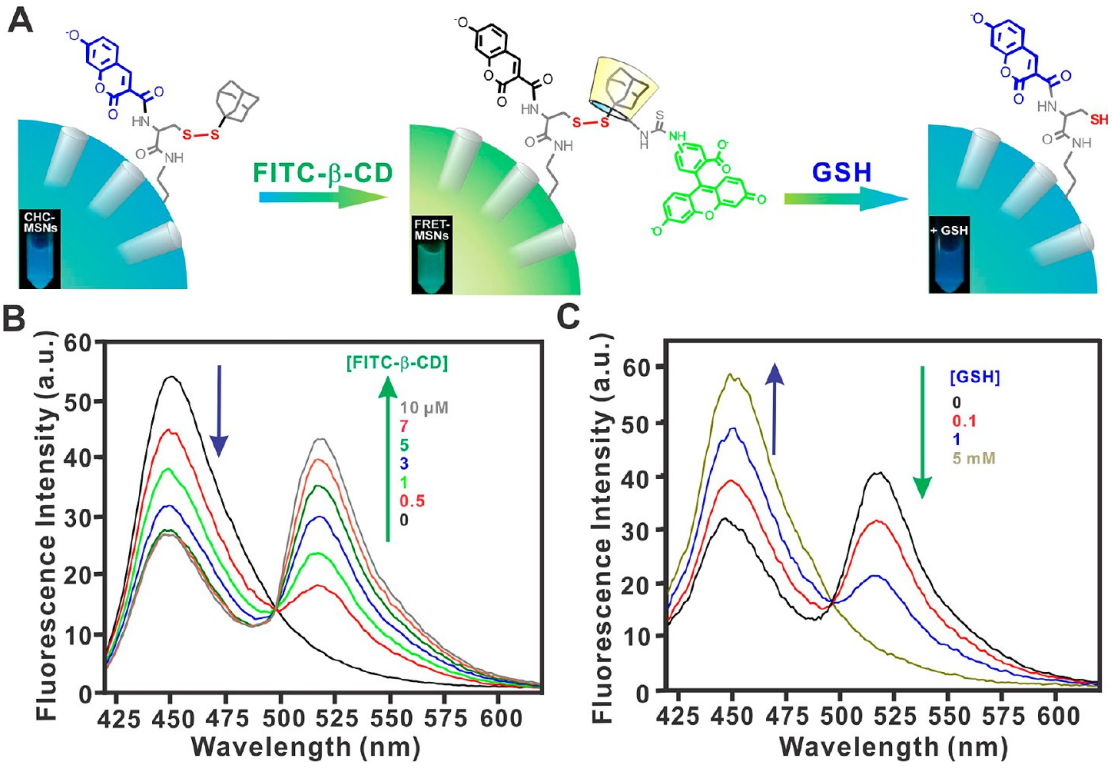

Figure 3. (A) Schematic diagram indicating the assembly of FRET-MSNs (left), upon addition of FITC-β-CD to CHC-MSNs; and subsequent cleavage of disulfide bond (right), following treatment of FRET-MSNs with glutathione (GSH). Inset figures show the corresponding change in color of the nanoparticle solution under a UV lamp (365 nm). (B) Changes in blue (450 nm) and green (520 nm) fluorescence upon addition of increasing concentrations of FITC-β-CD to the CHC-MSNs dispersed in pH 7.4 PBS, indicating formation of FRET-MSNs (FRET ON). (C) Changes in blue (450 nm) and green (520 nm) fluorescence upon addition of increasing GSH concentrations to FRET-MSNs dispersed in pH 7.4 PBS, indicating cleavage of disulfide bond (FRET OFF).

functionalized with 3-aminopropyltriethoxysilane (APTES) and grafted with *N*-Boc-cysteine *via* an amide bond. The thiol group of cysteine was conjugated with 1-adamantanethiol to form a redox-responsive disulfide bond, while the amine group was further labeled with 3-carboxy-7-hydroxyl-coumarin (CHC) to obtain the functional CHC-MSNs. Using transmission electron microscopy (TEM), we affirmed that the CHC-MSNs still retain the characteristics of MCM-41 type of MSNs, such as their spherical particle shape, having an average diameter of 100 $\pm$ 14 nm (n = 100) and hexagonally packed mesoporous structures (Figure 2B). This was also substantiated by N_2 adsorption isotherms which demonstrated that the CHC-MSNs have a Burnauer–Emmett–Teller (BET)-surface area of 398 $m^2 \cdot g^{-1}$ and a narrow Barrett–Joyner–Halenda (BJH) pore-size distribution (average pore diameter = 2.3 nm) (see Supporting Information, Figure S2). In addition, the cysteine functionalized MSNs show a characteristic Raman peak of free thiol group[51] at 2550 cm^{-1} (Figure 2C, top curve). However, after conjugation with 1-adamantanethiol *via* a disulfide bond, this characteristic free thiol peak disappeared, which confirmed the formation of a disulfide bond (Figure 2C bottom curve). Figure 2D shows the UV–vis absorption and fluorescence emission of CHC-MSNs, demonstrating the successful conjugation of CHC to the MSN surface and indicates that the CHC-moiety can act as the energy donor for FITC (see Supporting Information, Figure S4). Together with the FTIR characterization of CHC-MSNs (see Supporting Information, Figure S3), these results demonstrated the successful construction of CHC-MSNs.

Assembly of a Donor–Acceptor FRET Model. The synthesis of FRET-MSNs was then followed by the combination of the CHC-MSNs with FITC-β-CD *via* host–guest complexation between FITC-β-CD and adamantane moiety[52] present on CHC-MSNs (Figure 3A). As shown in Figure 2D, the coumarin moiety in CHC-MSNs can be excited by absorbing light with a wavelength of 405 nm, resulting in emission of light in the range of 430–480 nm. When the disulfide bond is intact (Figure 1), the coumarin moiety in CHC-MSNs upon excitation at 405 nm will act as a photon donor for the FITC-β-CD which absorbs maximally at 480 nm (see Supporting Information, Figure S4). We observed that the addition of FITC-β-CD leads to a decrease in blue fluorescence (450 nm) and an increase in green fluorescence (520 nm) (Figure 3B), which was also reflected in a significant change of the color of the solution from blue to green, sufficiently distinct to be identified *via* the naked eye (Figure 3A, inset). As seen in Figure 3B, further increases in the concentration of FITC-β-CD

quenched the blue fluorescence maximally. Additionally, from the data shown in Figure 3B, the ratio of relative fluorescence intensities (FRET signal R, where $R = F_{520\ nm}/F_{450\ nm}$) reached a value of 1.25 at a concentration of 3 μM for FITC-β-CD for a fixed concentration of CHC MSNs (10 $\mu g \cdot mL^{-1}$), which indicated the assembly of FITC-β-CD to the MSN surface reached a saturation point. Further addition of FITC-β-CD beyond the saturation point only led to an increase in the FITC fluorescence with negligible quenching of coumarin fluorescence, presumably due to the direct excitation of FITC at 405 nm.[46] When these nanoparticles were isolated from the solution and redispersed in PBS (pH 7.4), they displayed dual emission peaks at 450 and 520 nm upon excitation at 405 nm (see Supporting Information, Figure S5a). Collectively, these results demonstrated that FITC-β-CD can assemble onto the surface of the CHC-MSN surface through the formation of inclusion complex with 1-adamantanethiol, thereby inducing a donor−acceptor FRET system.

Redox-Responsive Behavior of FRET-MSNs. The redox-responsive property of the FRET-MSNs was examined by observing the changes in FRET signal in the presence of glutathione (GSH) which mimics the intracellular reducing environment (Figure 3A). As shown in Figure 3C, the addition of increasing concentrations of GSH (0.1−5 mM) to a buffered solution of FRET-MSNs induced a decrease in the green fluorescence (520 nm) accompanied by recovery of blue fluorescence (450 nm) upon excitation at 405 nm. This strongly indicated the cleavage of disulfide bond and the removal of the FRET acceptor, FITC-β-CD. Accordingly, the color of the solution changed from green to blue under UV lamp (365 nm) (Figure 3A, inset). Fluorescence spectrum of the isolated nanoparticles after redispersing in PBS (pH 7.4) revealed that these nanoparticles only show the emission at 450 nm (see Supporting Information, Figure S5b). On the basis of these results, we can confirm the redox-responsive behavior of our FRET-MSNs, which results in a concomitant change in the FRET signal.

Correlating Drug Release from FRET-MSNs to the FRET Signal. Once we confirmed the redox-responsive gating behavior of our FRET-MSNs, our next step was to utilize their FRET properties for monitoring the drug release from the pores. Since the modulation of FRET is integrated within the uncapping event, we hypothesize that the corresponding change in the FRET signal can be utilized for monitoring the drug release on a temporal level (Figure 4A). To demonstrate this, we chose doxorubicin (DOX) as our model cargo, which was loaded into the pores of MSNs by first mixing aqueous buffered solutions of CHC-MSNs and DOX for 12 h. Thereafter, the pores were capped with FITC-β-CD

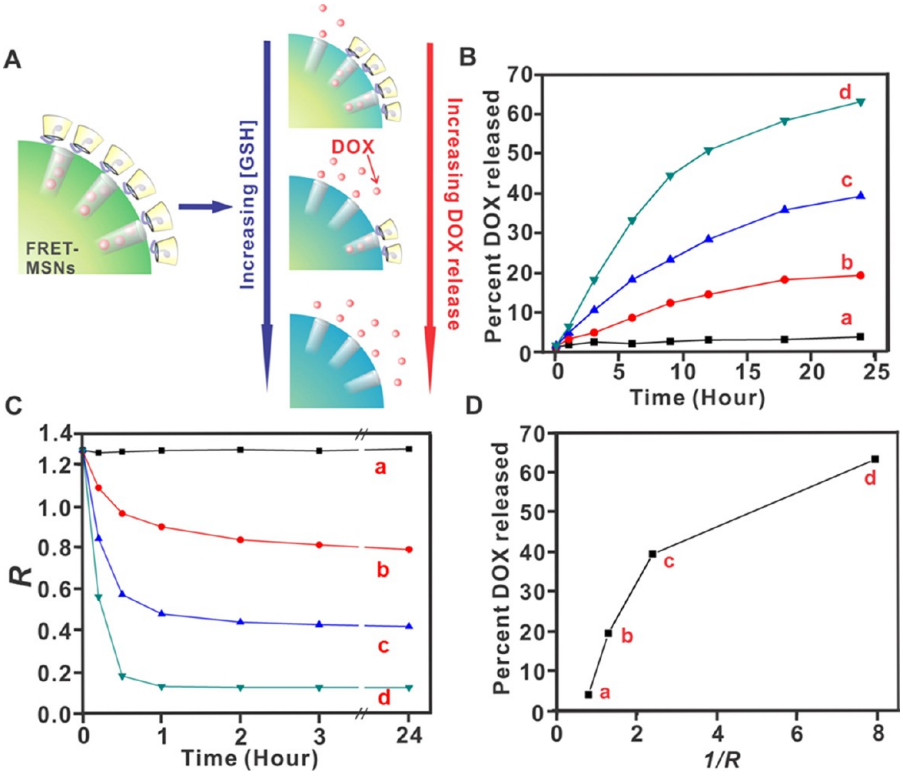

Figure 4. (A) Scheme showing the release of DOX at different concentrations of GSH and the corresponding change in FRET signal as well as color of FRET-MSNs. (B) Percent DOX released from the FRET-MSNs at different time points following treatment with increasing concentrations of GSH. (C) Change in FRET signal R at different time points following treatment of FRET-MSNs with increasing concentrations of GSH. (D) Correlation between percent DOX released and change in FRET signal R (plotted as $1/R$) at 24 h after GSH treatment. (a = no GSH, b = 0.1 mM GSH, c = 1 mM GSH, and d = 5 mM GSH).

and the final product (DOX-loaded FRET-MSNs) was isolated by centrifugation after repeated washing. The amount of DOX loaded into the pores of FRET-MSNs was determined to be 41.3 mg DOX/g of FRET-MSNs. It should be noted that the DOX-loaded FRET-MSNs were well-dispersed in aqueous solutions, owing to the presence of hydrophilic β-CD moieties on their surface, which can be exploited for the delivery of hydrophobic cargoes, like anticancer drugs.[53] To investigate the capping efficiency, DOX-loaded FRET-MSNs were dispersed in PBS (pH 7.4) and the absorbance of the released DOX in the absence of GSH was first monitored. As shown in Figure 4B (curve a), negligible release of DOX was observed over a period of 24 h, indicating that the FRET-MSNs remain intact in the absence of GSH. In contrast, the release profiles of DOX in the presence of varying concentrations of GSH depict an increase in the percent DOX released as time progressed (Figure 4B, curve b−d). From Figure 4B, we can see that the percent DOX released from the FRET-MSNs was dependent on GSH concentration, wherein concentrations of 0.1 mM or higher lead to significantly faster and greater release of DOX. Since the release of DOX only occurs when the pores are unlocked as a consequence of FITC-β-CD diffusing away from the FRET-MSNs, we also observed a corresponding change in the FRET signal *R*. As shown in Figure 4C, the addition of GSH (0.1 mM) to Dox-loaded FRET-MSNs induced a relatively slow time-dependent decrease in the FRET signal over a period of 3 h, while higher concentrations of GSH lead to a faster decrease in the FRET signal, reaching a minimal value of *R* within 1 h at 5 mM concentration of GSH. These GSH-concentration induced changes in the FRET signal remained constant over a period of 24 h, at which the release of DOX also reached a plateau. From this data (t = 24 h), a correlation between the amount of DOX released and FRET signal *R* was obtained (Figure 4D), which strongly suggested that the FRET-MSNs have the capability of monitoring the drug release in real-time.

Observing FRET Change in Cancer Cells Using FRET-MSNs. Prior to using the FRET-MSNs for cellular studies, we identified a range of concentrations within which the FRET-MSNs demonstrated minimal cytotoxicity (see Supporting Information, Figure S6). Using a cell proliferation assay, we found that concentrations lower than 20 $\mu g \cdot mL^{-1}$ induced negligible cytotoxicity in HeLa cells, and hence for all of our experiments, we utilized FRET-MSNs within this concentration range. To investigate the change in FRET signal following uptake and localization of FRET-MSNs in mammalian cells, we incubated the FRET-MSNs with cervical cancer cells (HeLa) and observed the change in FRET signal over extended periods of time (0−24 h) using confocal fluorescence microscopy. As seen in Figure 5A (top left), at time t = 0 h, blue-green spots were visible in the perinuclear region of HeLa cells when they were excited using 405 nm light, indicating intact FRET-MSNs with the FRET signal ON. From the emission spectrum (Figure 5A, top right), we can see that these spots show lower blue emission, but stronger green emission thus confirming that most of the FRET-MSNs were in the "FRET ON" stage at this time-point. However, at approximately t = 24 h, an increase in the blue fluorescence intensity and a corresponding decrease in the green fluorescence intensity (Figure 5A, bottom left) were observed when the cells were excited using 405 nm light. This was consistent with our expectation as the cleavage of disulfide bond would lead to the removal of FITC-β-CD cap, thereby leading to the recovery of the blue fluorescence intensity (Figure 5A, bottom right). The removal of the FITC-β-CD cap was further confirmed by observing diffuse FITC fluorescence throughout the cytoplasm, when the cells were excited using the FITC channel (488 nm) (see Supporting Information, Figure S8). These results demonstrated that we were able to monitor the change in the intracellular FRET signal over a period of time by using confocal microscopy.

As shown earlier, we have already demonstrated that our FRET-MSNs can respond to the presence of exogenous GSH by releasing the entrapped cargo with concurrent change in the FRET signal. However, to demonstrate this in mammalian cells, we used thioctic acid (TA, a GSH synthesis enhancer, 10 μM)[54] and *N*-ethylmaleimide (NEM, a GSH scavenger, 5 μM)[55,56] to modulate the intracellular GSH concentration. The HeLa cells were incubated with TA and NEM, 10 min prior to incubation with the FRET-MSNs and were subsequently analyzed using fluorescence microscopy. As depicted in Figure 5B, we observed a clear enhancement in the characteristic coumarin emission at 450 nm for the cells treated with TA in FRET channel (Ex = 405 nm), coupled with increased FITC fluorescence in FITC channel (Ex = 488 nm), indicating that higher number of the molecular valves (FITC-β-CD) were being removed from the surface of FRET-MSNs due to increased intracellular GSH concentration and were subsequently diffused into the cytoplasm. On the contrary, a distinct punctate blue-green fluorescence in the FRET channel, indicating FRET ON, was seen in the perinuclear region in case of cells treated with NEM. Since NEM decreases intracellular GSH concentration, there will be negligible cleavage and subsequent release of FITC-β-CD, hence resulting in the FRET being ON. As seen in Figure 5C, quantitative analysis of the relative intensities of coumarin emission (Ex = 405 nm. Em = 450 nm) also showed a similar trend of increasing coumarin emission as the intracellular GSH concentration increased. On the basis of these results, we were also able to confirm that the release of the molecular gate (FITC-β-CD) occurred in response to the redox stimuli, GSH present in millimolar levels in the cytoplasm of cancer cells.[43−45]

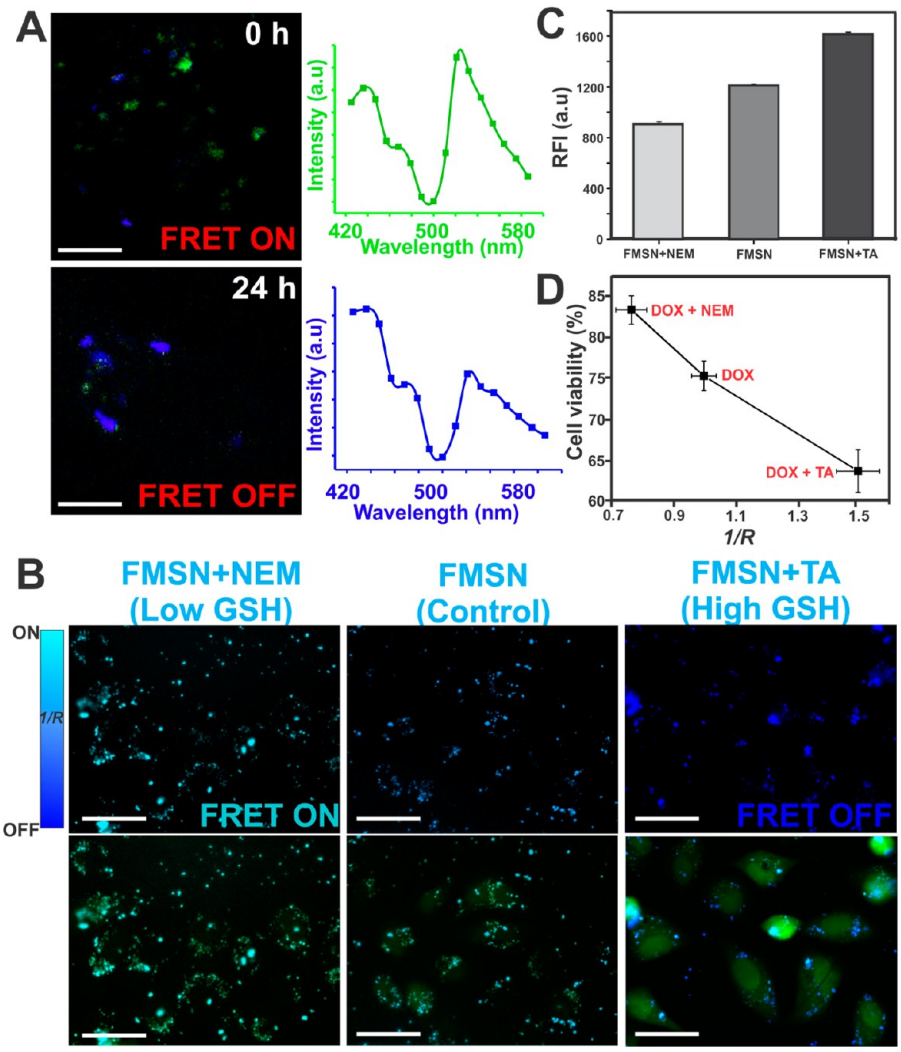

Figure 5. (A) Confocal microscopy images (left panel) depicting the change in FRET signal in HeLa cells treated with FRET-MSNs at different time points. Right panel shows the corresponding change in the average fluorescence intensities, when the cells were excited with 405 nm light (for more details see Supporting Information, Figure S7). Scale bar is 1 μm. (B) Fluorescence microscopy images showing the change in the fluorescence intensity (FRET channel, 405 nm excitation, top panel, and the merged images with FITC channel which used 488 nm as excitation, bottom panel) upon varying intracellular GSH concentration of HeLa cells, prior to treatment with FRET-MSNs. Cells treated with *N*-ethyl maleimide (NEM, 5 μM) present low levels of GSH, thereby FRET signal is on; whereas, the cells treated with thiotic acid (TA, 10 μM) have increased GSH levels and hence the FRET is turned off. The bar (top left corner) indicates the correlation between FRET signal *R* and the color of the FRET-MSNs seen in the top panel. Scale bar is 5 μm. (C) Quantitative comparison of the relative fluorescence intensities (RFI, Ex = 405 nm, Em = 450 nm), of the HeLa cells treated with TA and NEM. (D) Correlation between FRET signal *R* and cell viability, when the HeLa cells were treated with DOX loaded FRET-MSNs at varying GSH concentrations.

Monitoring Drug Release in Real-Time in Cancer Cells Using FRET-MSNs. However, it is important to demonstrate if we can correlate this change in the FRET signal with the corresponding drug release and its downstream therapeutic efficacy. To prove this, we treated HeLa cells with TA and NEM to modulate the cytoplasmic GSH concentration prior to the addition of DOX-loaded FRET-MSNs, and the viability of HeLa cells was monitored 24 h after treatment. The change in intracellular GSH concentration will result in a change in the extent of disulfide bond cleavage, which shall be displayed as a change in the FRET signal *R* as well as the amount of DOX released. Since the amount of DOX released from the nanoparticles influences the viability of cells, we can then correlate the change in FRET signal with the cell viability. As expected, the presence of TA, which increased the intracellular GSH concentration, led to an increase in the unlocking of pores which was associated with a decrease in the cell viability as well as an decrease in the FRET signal, *R* (thus 1/*R* increases as seen in Figure 5D, FRET OFF). In contrast, when the cells were pretreated with the GSH scavenger, NEM, we observed an increase in the cell viability as well as a increase in the FRET signal ratio, *R* (thus 1/*R* decreases as seen in Figure 5D, FRET ON). These results demonstrated the ability of our proposed FRET-MSNs based DDS in real-time monitoring drug release and reporting cell viability.

CONCLUSIONS

In summary, we have successfully demonstrated the formation of redox-responsive fluorescent MSNs, comprising an integrated FRET-based real-time monitoring system, which enabled tracking the release of the payload from the pores of the MSNs in real-time, by measuring the change in the FRET signal. We have shown a good correlation between the change in the FRET signal and the extent of drug released at different GSH concentrations both at the solution level as well as inside the cells. The advantage of our platform is that it can be extended to any cargo, fluorescent or nonfluorescent, as the molecular structures responsible for real-time monitoring are integrated within the unlocking mechanism present on the nanoparticle, and hence, we do not need to rely on the optical properties of the drug or a model dye. As such, we can monitor the release of the cargo on a temporal level, even if the drug is nonfluorescent, thus demonstrating the versatility of our platform. Additionally, no structural modification of the drug is required as the donor–acceptor pair is integrated within the nanoparticles, thereby preserving the drug efficacy. Numerous studies have demonstrated significantly higher intracellular glutathione concentrations in cancer cells as compared to normal cells, we can expect our FRET-MSNs to release the biomolecules more selectively in cancer cells. However, we can expect to extend the applications of the FRET-MSNs to any trigger such as pH or temperature by making appropriate structural modifications, since the FRET signal only depends on the donor–acceptor pair. Thus, we can envision our real-time monitoring system would provide a unique and universal strategy for overcoming the challenges encountered in the tracking (location) and monitoring (time) of drug release over extended periods of time and shows great potential for bioapplications, such as the investigation of cancer stem cells and effective therapies against them. However, a more advanced real-time monitoring system should also possess the capability of achieving direct monitoring of the release kinetics of drugs. Hence, we will explore additional avenues for enabling our FRET-MSNs to precisely monitor the kinetics of drug release as our future goals.

METHODS

Synthesis of FRET-MSNs. *NH_2-MSNs.*[50] In a typical synthesis procedure, 28 mg of sodium hydroxide and 100 mg of cetyl trimethyammonium bromide (CTAB) in sequence were completely dissolved into 50 mL of deionized water under vigorous stirring at 80 °C. After the solution became clear, 0.5 mL of TEOS was added dropwise in 10 min. After 3 h, 20 μL of APTES was added and the vigorous stirring was continued for 20 h, and then milk-white as-synthesized materials were collected by centrifugation. To remove the surfactant, the as-synthesized materials were refluxed in a solution consisting of 50 mL of ethanol and 0.5 mL of hydrochloric acid (36–38%) for 12 h, centrifuged and finally washed several times with methanol. The final products were dried for 12 h at 120 °C in vacuum.

Cys-MSNs. To a solution of *N*-Boc-cysteine (22 mg) and *N*-hydroxysuccinimide (NHS, 25 mg) in 5 mL of anhydrous DMF at 0 °C, 1-ethyl-3-(3-dimethylaminopropyl)carbodiimide hydrochloride (EDC·HCl, 31 mg) was added. The solution was stirred at 0 °C for 30 min and recovered to room temperature for additional 4 h. Then 100 mg of NH_2-MSNs in 5 mL of DMF solution was added slowly and the mixture was keep stirring overnight under N_2. The nanoparticles were collected by centrifugation and washed several times with DMF and methanol, and finally dried in vacuum to obtain Cys-MSNs.

Cys-TA-MSNs. A solution of Cys-MSNs (80 mg) in 5 mL of methanol was added dropwise into a solution of 2,2′-dithiodipyridine (0.1 g) in methanol/pH7.4 PBS solution (v/v, 10 mL/1.5 mL). The mixture was stirred at room temperature overnight and the nanoparticles were collected by centrifugation, washed thrice with methanol and finally redispersed in 10 mL of methanol. 1-Adamantanethiol (0.1 g) in 2 mL of methanol was then added to the above solution and the mixture was stirred overnight at room temperature under N_2 atmosphere. The Cys-TA-MSNs were collected by centrifugation, washed several times with methanol, and then dried under vacuum.

CHC-MSNs. A 5 mL portion of DCM solution of Cys-TA-MSNs (60 mg) was cooled to 0 °C for 30 min, and then 2 mL of trifluoroacetic acid (TFA) was added. The mixture was stirred at 0 °C for 30 min and then recovered to room temperature for an additional 3 h. Then 10 mL of methanol was added to dilute the mixture. The nanoparticles were collected by centrifugation and washed several times with methanol, dried in vacuum, and finally redispersed in 5 mL of anhydrous DMF. To a solution of 7-hydroxycoumarin-3-carboxylic acid (100 mg) and NHS (80 mg) in 5 mL of anhydrous DMF at 0 °C, 70 mg of EDC·HCl were added. The solution was stirred at 0 °C for 30 min and recovered to room temperature for an additional 4 h. Then, the 5 mL of DMF solution consisting of TFA-treated Cys-TA-MSN nanoparticles was added slowly to the solution and the mixture was keep for stirring overnight. The nanoparticles were collected by centrifugation and washed several times with DMF and methanol, and then finally dried in vacuum to obtain the CHC-MSNs.

Synthesis of FITC-β-CD. Mono-6-deoxy-6-amino-β-cyclodextrin (NH_2-β-CD) was first synthesized by a previously reported method.[57] ^{1}H NMR (300 MHz, D_2O): δ 4.97 (s, 7H), 3.74–3.88 (m), 3.38–3.56 (m), 3.08 (d, 1H, J = 14.2 Hz), 2.84 (dd, 1H, $J1$ = 7.0 Hz, $J2$ = 14.1 Hz). ESI-MS m/z 1132.3 $[M\text{-}H]^-$. An amount of 38 mg of FITC along with 10 mg of DMAP and 0.1 g of NH_2-β-CD was added into 5 mL anhydrous DMF and the solution was stirred overnight at room temperature under N_2. A 10 mL portion of acetone was added to the solution and the precipitate was collected and washed with acetone several times. ESI-MS m/z 1521.9 $[M\text{-}H]^-$, 761.3 $[M\text{-}2H]/2^-$.

Characterizations. UV–vis absorption spectra were recorded on a Varian Cary 50 spectrophotometer. Fluorescence spectra were recorded on a Varian Cary Eclipse fluorescence spectrophotometer. FT-IR spectra were collected on an Avatar Nicolet FT-IR330 spectrometer. Raman spectrum characterizations were performed on Laser Raman, Renishaw inVia Raman microscope. ^{1}H NMR was acquired on Varian 300 MHz NMR spectrometer. ESI-MS was collected on Finnigan LCQ DUO LC/MS spectrometer. TEM was performed on a Topcon 002B electron microscope at 200 kV. Sample preparation was carried out by placing a drop of the freshly prepared colloidal solution on a carbon-coated copper grid and allowing the solution to evaporate. Nitrogen adsorption–desorption measurements were performed on a Micromeritics Tristar-3000 surface area analyzer at −196 °C. The sample was dried at 200 °C for 3 h before analysis. The BET specific surface areas were calculated using the first 10 experimental data points. Pore volumes were determined from the amount of N_2 adsorbed at the single point, P/P_0 = 0.98.

Cell-Lines and Culture. HeLa cells were used for FRET-MSNs. HeLa cells were cultured in DMEM supplemented with 10% FBS and 1% streptomycin−penicillin. For the delivery experiment, passaged cells were prepared to 40−60% confluency in 24-well plates. After 24 h of plating, media was exchanged with serum-free basal media (500 μL) and FRET-MSNs/X-tremeGENE complexes (50 μL) were added. After incubation for 6 h, media was exchanged with normal growth medium. Fluorescence measurements were performed after 0−24 h after transfection.

Imaging of FRET-MSNs. At different time points following transfection, the cells were imaged using fluorescent microscopy. The effect of GSH concentration on the FRET signal was studied using the epifluorescence microscopy. For this purpose, the fluorescent and phase contrast images were obtained using the Nikon T2500 inverted epifluorescence microscope. Each image was captured with different channels and focus. Images were processed and overlapped using Image-Pro (Media Cybernetics) and ImageJ (NIH). To monitor and quantify the change in FRET signal *in vitro*, confocal imaging was done using a Zeiss LSM 510-META confocal microscope equipped with an Axiovert 200 inverted Scope.

Conflict of Interest: The authors declare no competing financial interest.

Acknowledgment. K.B.L. acknowledges the support from the NIH Director's Innovator Award (1DP20D006462-01), Rutgers Faculty Research Grant (281673), and the NJ Commission on the Spinal Cord Grant (09-3085-SCR-E-0). We thank Prof. Tewodros Asefa for support in BET analysis, Benjamin Groth for assistance in Raman microscopy, and Dr. Zui Pan for providing help in confocal imaging. We also thank KBLEE group members for their valuable suggestions for the project.

Supporting Information Available: Nitrogen adsorption−desorption isotherms, FTIR spectrum, UV−vis absorption spectrum, ^{1}H NMR and ESI-MS characterization of the MSNs and CDs, and cell viability assay of FRET-MSNs. This material is available free of charge *via* the Internet at http://pubs.acs.org.

REFERENCES AND NOTES

1. Vaupel, P.; Kallinowski, F.; Okunieff, P. Blood-Flow, Oxygen and Nutrient Supply, and Metabolic Microenvironment of Human-Tumors—A Review. *Cancer Res.* **1989**, *49*, 6449–6465.
2. Sidransky, D. Emerging Molecular Markers of Cancer. *Nat. Rev. Cancer* **2002**, *2*, 210–219.
3. Tennant, D. A.; Duran, R. V.; Gottlieb, E. Targeting Metabolic Transformation for Cancer Therapy. *Nat. Rev. Cancer* **2010**, *10*, 267–277.
4. Li, J. M.; Wang, Y. Y.; Zhao, M. X.; Tan, C. P.; Li, Y. Q.; Le, X. Y.; Ji, L. N.; Mao, Z. W. Multifunctional QD-Based Co-delivery of siRNA and Doxorubicin to HeLa Cells for Reversal of Multidrug Resistance and Real-Time Tracking. *Biomaterials* **2012**, *33*, 2780–2790.
5. Shen, J. A.; Yin, Q.; Chen, L. L.; Zhang, Z. W.; Li, Y. P. Co-delivery of Paclitaxel and Survivin shRNA by Pluronic P85-PEI/TPGS Complex Nanoparticles to Overcome Drug Resistance in Lung Cancer. *Biomaterials* **2012**, *33*, 8613–8624.
6. Xiong, X. B.; Lavasanifar, A. Traceable Multifunctional Micellar Nanocarriers for Cancer-Targeted Co-delivery of MDR-1 siRNA and Doxorubicin. *ACS Nano* **2011**, *5*, 5202–5213.
7. Zhou, J. B.; Liu, J.; Cheng, C. J.; Patel, T. R.; Weller, C. E.; Piepmeier, J. M.; Jiang, Z. Z.; Saltzman, W. M. Biodegradable Poly(amine-co-ester) Terpolymers for Targeted Gene Delivery. *Nat. Mater.* **2012**, *11*, 82–90.
8. Delcea, M.; Yashchenok, A.; Videnova, K.; Kreft, O.; Mohwald, H.; Skirtach, A. G. Multicompartmental Micro- and Nanocapsules: Hierarchy and Applications in Biosciences. *Macromol. Biosci.* **2010**, *10*, 465–474.
9. Huang, W. C.; Hu, S. H.; Liu, K. H.; Chen, S. Y.; Liu, D. M. A Flexible Drug Delivery Chip for the Magnetically-Controlled Release of Anti-epileptic Drugs. *J. Controlled Release* **2009**, *139*, 221–228.
10. Klaikherd, A.; Nagamani, C.; Thayumanavan, S. Multi-stimuli Sensitive Amphiphilic Block Copolymer Assemblies. *J. Am. Chem. Soc.* **2009**, *131*, 4830–4838.
11. Lux, C. D.; Joshi-Barr, S.; Nguyen, T.; Mahmoud, E.; Schopf, E.; Fomina, N.; Almutairi, A. Biocompatible Polymeric Nanoparticles Degrade and Release Cargo in Response to Biologically Relevant Levels of Hydrogen Peroxide. *J. Am. Chem. Soc.* **2012**, *134*, 15758–15764.
12. Schmaljohann, D. Thermo- and pH-responsive Polymers in Drug Delivery. *Adv. Drug. Delivery Rev.* **2006**, *58*, 1655–1670.
13. Wong, A. D.; DeWit, M. A.; Gillies, E. R. Amplified Release through the Stimulus Triggered Degradation of Self-Immolative Oligomers, Dendrimers, and Linear Polymers. *Adv. Drug. Delivery Rev.* **2012**, *64*, 1031–1045.
14. Nakanishi, J.; Nakayama, H.; Shimizu, T.; Ishida, H.; Kikuchi, Y.; Yamaguchi, K.; Horiike, Y. Light-Regulated Activation of Cellular Signaling by Gold Nanoparticles That Capture and Release Amines. *J. Am. Chem. Soc.* **2009**, *131*, 3822–3823.
15. Delcea, M.; Mohwald, H.; Skirtach, A. G.; Stimuli-Responsive, L. B. L. Capsules and Nanoshells for Drug Delivery. *Adv. Drug. Delivery Rev.* **2011**, *63*, 730–747.
16. Jana, A.; Devi, K. S. P.; Maiti, T. K.; Singh, N. D. P. Perylene-3-yl-methanol: Fluorescent Organic Nanoparticles as a Single-Component Photoresponsive Nanocarrier with Real-Time Monitoring of Anticancer Drug Release. *J. Am. Chem. Soc.* **2012**, *134*, 7656–7659.
17. Lee, M. H.; Kim, J. Y.; Han, J. H.; Bhuniya, S.; Sessler, J. L.; Kang, C.; Kim, J. S. Direct Fluorescence Monitoring of the Delivery and Cellular Uptake of a Cancer-Targeted RGD Peptide-Appended Naphthalimide Theragnostic Prodrug. *J. Am. Chem. Soc.* **2012**, *134*, 12668–12674.
18. Ock, K.; Jeon, W. I.; Ganbold, E. O.; Kim, M.; Park, J.; Seo, J. H.; Cho, K.; Joo, S. W.; Lee, S. Y. Real-Time Monitoring of Glutathione-Triggered Thiopurine Anticancer Drug Release in Live Cells Investigated by Surface-Enhanced Raman Scattering. *Anal. Chem.* **2012**, *84*, 2172–2178.
19. Santra, S.; Kaittanis, C.; Santiesteban, O. J.; Perez, J. M. Cell-Specific, Activatable, and Theranostic Prodrug for Dual-Targeted Cancer Imaging and Therapy. *J. Am. Chem. Soc.* **2011**, *133*, 16680–16688.
20. Weinstain, R.; Segal, E.; Satchi-Fainaro, R.; Shabat, D. Real-Time Monitoring of Drug Release. *Chem. Commun.* **2010**, *46*, 553–555.
21. Cui, W.; Lu, X. M.; Cui, K.; Wu, J.; Wei, Y.; Let, Q. H. Fluorescent Nanoparticles of Chitosan Complex for Real-Time Monitoring Drug Release. *Langmuir* **2011**, *27*, 8384–8390.
22. Vivero-Escoto, J. L.; Slowing, I. I.; Trewyn, B. G.; Lin, V. S. Y. Mesoporous Silica Nanoparticles for Intracellular Controlled Drug Delivery. *Small* **2010**, *6*, 1952–1967.
23. Tang, F. Q.; Li, L. L.; Chen, D. Mesoporous Silica Nanoparticles: Synthesis, Biocompatibility and Drug Delivery. *Adv. Mater.* **2012**, *24*, 1504–1534.
24. Asefa, T.; Tao, Z. M. Biocompatibility of Mesoporous Silica Nanoparticles. *Chem. Res. Toxicol.* **2012**, *25*, 2265–2284.
25. Angelos, S.; Yang, Y. W.; Khashab, N. M.; Stoddart, J. F.; Zink, J. I. Dual-Controlled Nanoparticles Exhibiting AND Logic. *J. Am. Chem. Soc.* **2009**, *131*, 11344–11346.
26. Fang, W. J.; Yang, J.; Gong, J. W.; Zheng, N. F. Photo- and pH-Triggered Release of Anticancer Drugs from Mesoporous Silica-Coated Pd@Ag Nanoparticles. *Adv. Funct. Mater.* **2012**, *22*, 842–848.
27. Ferris, D. P.; Zhao, Y. L.; Khashab, N. M.; Khatib, H. A.; Stoddart, J. F.; Zink, J. I. Light-Operated Mechanized Nanoparticles. *J. Am. Chem. Soc.* **2009**, *131*, 1686–1688.
28. Lai, J. P.; Mu, X.; Xu, Y. Y.; Wu, X. L.; Wu, C. L.; Li, C.; Chen, J. B.; Zhao, Y. B. Light-Responsive Nanogated Ensemble Based on Polymer Grafted Mesoporous Silica Hybrid Nanoparticles. *Chem. Commun.* **2010**, *46*, 7370–7372.
29. Lin, Q. N.; Huang, Q.; Li, C. Y.; Bao, C. Y.; Liu, Z. Z.; Li, F. Y.; Zhu, L. Y. Anticancer Drug Release from a Mesoporous Silica Based Nanophotocage Regulated by Either a One- or Two-Photon Process. *J. Am. Chem. Soc.* **2010**, *132*, 10645–10647.

30. Liu, C. Y.; Guo, J.; Yang, W. L.; Hu, J. H.; Wang, C. C.; Fu, S. K. Magnetic Mesoporous Silica Microspheres with Thermo-Sensitive Polymer Shell for Controlled Drug Release. *J. Mater. Chem.* **2009**, *19*, 4764–4770.
31. Ma, M.; Chen, H. R.; Chen, Y.; Wang, X.; Chen, F.; Cui, X. Z.; Shi, J. L. Au Capped Magnetic Core/Mesoporous Silica Shell Nanoparticles for Combined Photothermo-/chemo-Therapy and Multimodal Imaging. *Biomaterials* **2012**, *33*, 989–998.
32. Tian, B. S.; Yang, C. Thermo-Sensitive Poly(*N*-isopropylacrylamide)/Mesoporous Silica Nanocomposites as Controlled Delivery Carriers: Loading and Release Behaviors for Drug Ibuprofen. *J. Nanosci. Nanotechno.* **2011**, *11*, 1871–1879.
33. Angelos, S.; Yang, Y. W.; Patel, K.; Stoddart, J. F.; Zink, J. I. pH-Responsive Supramolecular Nanovalves Based on Cucurbit[6]uril Pseudorotaxanes. *Angew. Chem., Int. Ed.* **2008**, *47*, 2222–2226.
34. Park, C.; Oh, K.; Lee, S. C.; Kim, C. Controlled Release of Guest Molecules from Mesoporous Silica Particles Based on a pH-Responsive Polypseudorotaxane Motif. *Angew. Chem., Int. Ed.* **2007**, *46*, 1455–1457.
35. Angelos, S.; Khashab, N. M.; Yang, Y. W.; Trabolsi, A.; Khatib, H. A.; Stoddart, J. F.; Zink, J. I. pH Clock-Operated Mechanized Nanoparticles. *J. Am. Chem. Soc.* **2009**, *131*, 12912–12914.
36. Liu, R.; Zhang, Y.; Zhao, X.; Agarwal, A.; Mueller, L. J.; Feng, P. Y. pH-Responsive Nanogated Ensemble Based on Gold-Capped Mesoporous Silica through an Acid-Labile Acetal Linker. *J. Am. Chem. Soc.* **2010**, *132*, 1500–1501.
37. Lee, C. H.; Cheng, S. H.; Huang, I. P.; Souris, J. S.; Yang, C. S.; Mou, C. Y.; Lo, L. W. Intracellular pH-Responsive Mesoporous Silica Nanoparticles for the Controlled Release of Anticancer Chemotherapeutics. *Angew. Chem., Int. Ed.* **2010**, *49*, 8214–8219.
38. Singh, N.; Karambelkar, A.; Gu, L.; Lin, K.; Miller, J. S.; Chen, C. S.; Sailor, M. J.; Bhatia, S. N. Bioresponsive Mesoporous Silica Nanoparticles for Triggered Drug Release. *J. Am. Chem. Soc.* **2011**, *133*, 19582–19585.
39. Climent, E.; Martinez-Manez, R.; Sancenon, F.; Marcos, M. D.; Soto, J.; Maquieira, A.; Amoros, P. Controlled Delivery Using Oligonucleotide-Capped Mesoporous Silica Nanoparticles. *Angew. Chem., Int. Ed.* **2010**, *49*, 7281–7283.
40. Climent, E.; Bernardos, A.; Martinez-Manez, R.; Maquieira, A.; Marcos, M. D.; Pastor-Navarro, N.; Puchades, R.; Sancenon, F.; Soto, J.; Amoros, P. Controlled Delivery Systems Using Antibody-Capped Mesoporous Nanocontainers. *J. Am. Chem. Soc.* **2009**, *131*, 14075–14080.
41. Park, C.; Kim, H.; Kim, S.; Kim, C. Enzyme Responsive Nanocontainers with Cyclodextrin Gatekeepers and Synergistic Effects in Release of Guests. *J. Am. Chem. Soc.* **2009**, *131*, 16614–16615.
42. Popat, A.; Ross, B. P.; Liu, J.; Jambhrunkar, S.; Kleitz, F.; Qiao, S. Z. Enzyme-Responsive Controlled Release of Covalently Bound Prodrug from Functional Mesoporous Silica Nanospheres. *Angew. Chem., Int. Ed.* **2012**, *51*, 12486–12489.
43. Cheng, R.; Feng, F.; Meng, F. H.; Deng, C.; Feijen, J.; Zhong, Z. Y. Glutathione-Responsive Nano-vehicles as a Promising Platform for Targeted Intracellular Drug and Gene Delivery. *J. Controlled Release* **2011**, *152*, 2–12.
44. Balendiran, G. K.; Dabur, R.; Fraser, D. The Role Of Glutathione in Cancer. *Cell. Biochem. Funct.* **2004**, *22*, 343–352.
45. Wang, Y. C.; Wang, F.; Sun, T. M.; Wang, J. Redox-Responsive Nanoparticles from the Single Disulfide Bond-Bridged Block Copolymer as Drug Carriers for Overcoming Multidrug Resistance in Cancer Cells. *Bioconjugate Chem.* **2011**, *22*, 1939–1945.
46. Lakowicz, J. R. *Principles of Fluorescence Spectroscopy*; 3rd ed.; Springer: Singapore, 2006.
47. Bagalkot, V.; Zhang, L.; Levy-Nissenbaum, E.; Jon, S.; Kantoff, P. W.; Langer, R.; Farokhzad, O. C. Quantum Dot-Aptamer Conjugates for Synchronous Cancer Imaging, Therapy, and Sensing of Drug Delivery Based on Bi-fluorescence Resonance Energy Transfer. *Nano Lett.* **2007**, *7*, 3065–3070.
48. Ho, Y.-P.; Chen, H. H.; Leong, K. W.; Wang, T.-H. Evaluating the Intracellular Stability and Unpacking of DNA Nanocomplexes by Quantum Dots-FRET. *J. Controlled Release* **2006**, *116*, 83–89.
49. Jung, J. J.; Solanki, A.; Memoli, K. A.; Kamei, K.; Kim, H.; Drahl, M. A.; Williams, L. J.; Tseng, H. R.; Lee, K. Selective Inhibition of Human Brain Tumor Cells through Multifunctional Quantum-Dot-Based siRNA Delivery. *Angew. Chem., Int. Ed.* **2010**, *49*, 103–107.
50. He, Q. J.; Zhang, J. M.; Shi, J. L.; Zhu, Z. Y.; Zhang, L. X.; Bu, W. B.; Guo, L. M.; Chen, Y. The Effect of Pegylation of Mesoporous Silica Nanoparticles on Nonspecific Binding of Serum Proteins and Cellular Responses. *Biomaterials* **2010**, *31*, 1085–1092.
51. Sauer, A. M.; Schlossbauer, A.; Ruthardt, N.; Cauda, V.; Bein, T.; Brauchle, C. Role of Endosomal Escape for Disulfide-Based Drug Delivery from Colloidal Mesoporous Silica Evaluated by Live-Cell Imaging. *Nano Lett.* **2010**, *10*, 3684–3691.
52. Szejtli, J. Introduction and General Overview of Cyclodextrin Chemistry. *Chem. Rev.* **1998**, *98*, 1743–1753.
53. Kim, C.; Shah, B. P.; Subramaniam, P.; Lee, K. B. Synergistic Induction of Apoptosis in Brain Cancer Cells by Targeted Codelivery of siRNA and Anticancer Drugs. *Mol. Pharm.* **2011**, *8*, 1955–1961.
54. Deng, R.; Xie, X.; Vendrell, M.; Chang, Y.-T.; Liu, X. Intracellular Glutathione Detection Using MnO_2-Nanosheet-Modified Upconversion Nanoparticles. *J. Am. Chem. Soc.* **2011**, *133*, 20168–20171.
55. Gao, W.; Langer, R.; Farokhzad, O. C. Poly(ethylene glycol) with Observable Shedding. *Angew. Chem., Int. Ed.* **2010**, *49*, 6567–6571.
56. Yang, J.; Chen, H.; Vlahov, I. R.; Cheng, J. X.; Low, P. S. Evaluation of Disulfide Reduction during Receptor-Mediated Endocytosis by using FRET Imaging. *Proc. Natl. Acad. Sci. U.S.A.* **2006**, *103*, 13872–13877.
57. Tang, W.; Ng, S. C. Facile Synthesis of Mono-6-Amino-6-Deoxy-Alpha-, Beta-, Gamma-Cyclodextrin Hydrochlorides for Molecular Recognition, Chiral Separation and Drug Delivery. *Nat. Protoc.* **2008**, *3*, 691–697.